Colloids and Surfaces B: Biointerfaces 187 (2020) 110609

Contents lists available at ScienceDirect

Colloids and Surfaces B: Biointerfaces

journal homepage: www.elsevier.com/locate/colsurfb

Lipid shape determination of detergent solubilization in mixed-lipid liposomes

Samantha T. Clark[a], Matthias M.L. Arras[b,1], Stephen A. Sarles[c], Paul D. Frymier[a,*]

[a] Department of Chemical and Biomolecular Engineering, University of Tennessee, Knoxville, 1512 Middle Dr, Knoxville, TN 37996, USA
[b] Neutron Scattering Division, Oak Ridge National Laboratory, Oak Ridge, TN 37831, USA
[c] Department of Mechanical, Aerospace, and Biomedical Engineering, University of Tennessee, 1512 Middle Drive, 414 Dougherty Engineering Building, Knoxville, TN 37996, USA

ARTICLE INFO

Keywords:
Lipid shape
Detergent-mediated liposome solubilization
Mixed-lipid liposomes
Egg phosphatidic acid (ePA)
Egg phosphatidylcholine (ePC)
Triton X-100 (TX)

ABSTRACT

The effects of lipid charge and head group size on liposome partitioning by detergents is an important consideration for applications such as liposomal drug delivery or proteoliposome formation. Yet, the solubilization of mixed-lipid liposomes, those containing multiple types of lipids, by detergents has received insufficient attention. This study examines the incorporation into and subsequent dissolution of mixed-lipid liposomes comprised of both egg phosphatidylcholine (ePC) and egg phosphatidic acid (ePA) by the detergent Triton-X100 (TX). Liposomes were prepared with mixtures of the two lipids, ePC and ePA, at molar ratios from 0 to 1, then step-wise solubilized with TX. Changes in turbidity, size distribution, and molar heat power at constant temperature throughout the solubilization process were assessed. The data suggest that the difference in lipid shapes (shape factors = 0.74 and 1.4 [1,2]) affects packing in membranes, and hence influences how much TX can be incorporated before disruption. As such, liposomes containing the observed ratios of ePA incorporated higher concentrations of TX before initiating dissolution into detergent and lipid mixed-micelles. The cause was concluded to be increased mismatching in the bilayer from the conical shape of ePA compared to the cylindrical shape of ePC. Additionally, the degree to which ePA is approximated as conical versus cylindrical was modulated with pH. It was confirmed that less conical ePA behaved more similarly to ePC than more conical ePA. The understanding gained here on lipid shape in liposome incorporation of TX enables research to use *in vitro* liposomes that more closely mimic native membranes.

1. Introduction

Previous work in our lab utilizes the membrane protein Photosystem I (PSI) [3–7] found in plants, algae, and photosynthetic bacteria to initiate charge-separation upon illumination. To increase the photoactivity of PSI, we require methods to incorporate this protein into liposomes, which are similar to the protein's native environment. A common method used for the insertion of large membrane proteins such as PSI into liposomes is detergent-mediated reconstitution [8–10]. In this method, liposomes are saturated with detergent molecules (at detergent-to-lipid mass ratio R_{sat}) to disrupt lipid–lipid interactions and ease incorporation of proteins into the membranes. Disruption of the liposomes via detergent is commonly referred to as liposome solubilization. There is an optimum stage of liposome disruption for protein incorporation, dependent on the detergent-to-lipid ratio (D:L), beyond which liposomes are fully disrupted into micelles containing a mixture of lipid and detergent molecules (at detergent-to-lipid mass ratio R_{sol}) [11–14]. Previous research has investigated a wide range of interactions between lipids, like phosphatidylcholine (PC), phosphatidic acid (PA), and phosphatidylglycerol (PG), and detergents, like Triton X-100 (TX), dodecyl maltoside, octyl glucoside, and cholamidopropyl dimethylammonio propanesulfonate both experimentally [15–21,8], and using

* Corresponding author.
E-mail address: pdf@utk.edu (P.D. Frymier).
[1] Present Address: DSM, Materials Science Center, Urmonderbaan 22, 6167RD Geleen, The Netherlands.

https://doi.org/10.1016/j.colsurfb.2019.110609
Received 25 June 2019; Received in revised form 17 September 2019; Accepted 21 October 2019
Available online 10 November 2019

computational molecular dynamic simulations [22,23]. Amongst these, a common mechanism has been elucidated that describes detergent-liposome interactions in a three-stage model [12,24,25]. This model is explained in detail in Section 2.3.

Despite extensive knowledge on single lipid and single detergent mixtures, little is known about how mixtures of lipid types in mixed-lipid liposomes influence detergent solubilization. Insights into these interactions will better enable protein reconstitution into liposomes that more closely resemble native membrane lipid mixtures in order to enhance protein stability and function [10]. One system of mixed-lipid liposomes made of 16:0PC and 16:0PG has been solubilized with bile salt [21], yet more systems need to be understood.

In this study, we examine interactions of the detergent, TX, with mixed-lipid liposomes made with varying ratios of egg PC (ePC) and egg PA (ePA) lipids. These lipids were chosen because they have been used to successfully incorporate PSI into mixed-lipid liposomes with a fixed 9:1 ratio of ePC:ePA [26]. Despite initial success there is need to utilize higher ratios of ePA to more closely mimic the charge composition of the cyanobacterial thylakoid membrane in which PSI is located [27].

Additionally, PC is a relevant test lipid because it is commonly used in *in vitro* applications, and it is a nonionic phospholipid that is the most abundant lipid in the majority of cell membranes [16]. Here, the inclusion of PA represents the negatively charged lipid fraction, which typically composes 10–20% of the lipids in *in vivo* membranes [28]. From a physical chemistry standpoint, these lipids are interesting because the shape of ePC is cylindrical in the bilayer and the shape of ePA is conical in the bilayer under physiological conditions [29]. The shape factor, which is the hydrocarbon volume divided by the optimal head area and the critical chain length, of each of these lipids is 0.74 and 1.4, respectively [1,2,29]. Furthermore, the degree of ionization of the PA head group can be easily modulated with pH [30–32]. The ionization changes the volume of the counterions associated with the PA head group, and therefore the cone angle of the lipids in the bilayer. The shapes, structures and ionization potentials of PC and PA are shown in Fig. 1. The lipids are representatively depicted with two acyl chains that each consist of an 18-carbon chain and 1 unsaturated bond (18:1), which is one of the main fatty acids present in naturally occurring ePC and ePA (Table S1). In addition to the successful use of ePC and ePA in reconstituting PSI mentioned above [26], naturally occurring lipids were selected because they better simulate the heterogeneity of *in vivo* membranes, which contain many lipids types and a diverse assortment of fatty acid chains. To our knowledge, no systematic study of detergent solubilization with ePC and ePA mixed-lipid liposomes at varying headgroup ratios has been performed.

Using absorbance spectrometry, dynamic light scattering, and isothermal titration calorimetry, we identified D:L ratios at which phase transitions occur for detergent reconstitution of ePC:ePA mixed-lipid liposomes. We observed the TX concentration at R_{sat} and R_{sol} significantly increases when the concentration of ePA in the liposomes is greater than 25%. The difference in lipid shape provides explanation: ePA lipids, which have conical molecular shapes, form defect-rich bilayers that facilitate greater incorporation of TX. Conversely, ePC lipids have cylindrical shapes that favor increased areas of contact with adjacent lipids and result in a lower probability of TX insertion. Additionally, we examined the influence of headgroup charge on TX solubilization of ePA membranes and determined that a more negative net charge results in decreases in TX concentration at R_{sat} and R_{sol}. We further apply the shape model to explain that as negative charges increase, there is a concomitant increase in counter-ions that increases the effective head group size and decreases mismatch in the ePA bilayer.

2. Materials and methods

2.1. Materials

Potassium phosphate, sodium sulfate, and potassium sulfate were purchased from Fisher Scientific to prepare aqueous buffer solutions of 25 mM KH_2PO_4-KOH pH 7, 50 mM Na_2SO_4, 50 mM K_2SO_4 in ultrapure de-ionized water. Lipid derivatives from chicken eggs of phosphatidylcholine (ePC) and phosphatidic acid (ePA) were purchased from Avanti Polar Lipids, Inc. as powders with purity greater than 99%. Additionally, powder lipids, 1,2-dipalmitoyl-sn-glycero-3-phosphocholine (16:0PC) and 1,2-dipalmitoyl-sn-glycero-3-phosphate (sodium salt) (16:0PA), were also purchased from Avanti Polar Lipids, Inc. at greater than 99% purity. 16:0PC and 16:0PA are purified lipids of the predominant fatty acid chain in egg of both PC and PA. The detergent, Triton X-100 (< 3% polyethylene glycol), was purchased from Sigma–Aldrich, as was chloroform (99.8% pure) used to solvate the lipid powders. All compounds were used without further purification. Fig. 1 shows some basic properties of the lipids PC and PA. The fatty acid saturation distribution of ePC and ePA derivatives is within 1.5% deviation identical, as seen in Table S1.

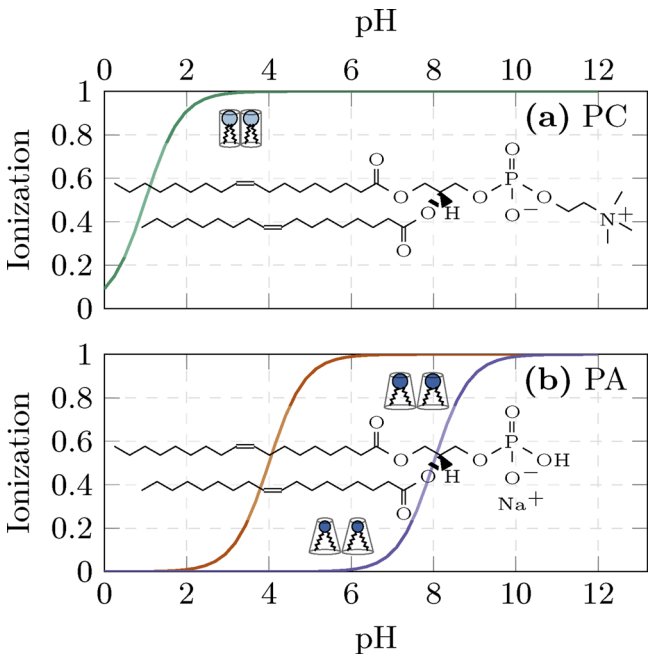

Fig. 1. (a) Chemical and shape structures of phosphatidylcholine (PC) and (b) phosphatidic acid (PA) lipids are shown overlaying the ionization potential of the lipids with $pK_a \approx 1$ (——), $pK_a = 4$ (——), $pK_a = 8$ (——). Due to the nature of the lipid head groups, the overall lipid shape of PC approximates a cylinder and that of PA approximates a cone. Increasing pH along the pK_a curve increases the net negative charge of the lipids, and thus the number of counter ions associated with the head group. This changes the shape of PA lipids from more to less conical.

2.2. Liposome preparation

Lipid powders were suspended in chloroform, then mixed at the desired mass-to-mass ratios and aliquoted in small glass flasks. The chloroform was completely evaporated overnight in a vacuum desiccator to form a thin lipid film on the flask walls. For the mixed-lipid liposome samples, the lipids were mixed together in inorganic solvent at the appropriate ratios prior to solvent evaporation. All lipid films were hydrated at 20 mg/mL in potassium phosphate buffer pH 7.2 (25 mM KH_2PO_4-KOH pH 7, 50 mM Na_2SO_4, 50 mM K_2SO_4). Vials were vortexed on low with a Fisher Scientific analog vortex mixer and heated 10 °C above the known phase transition temperature for 10 min to form multi-lamellar vesicles (MLVs) [33]. MLV solutions were put through 4 freeze-thaw cycles between −20 °C and room temperature. The stock lipids were mixed and diluted to 4 mg/mL with potassium phosphate buffer at pH 4.6, 7.2, or 10.2 for use. The liposomes were extruded

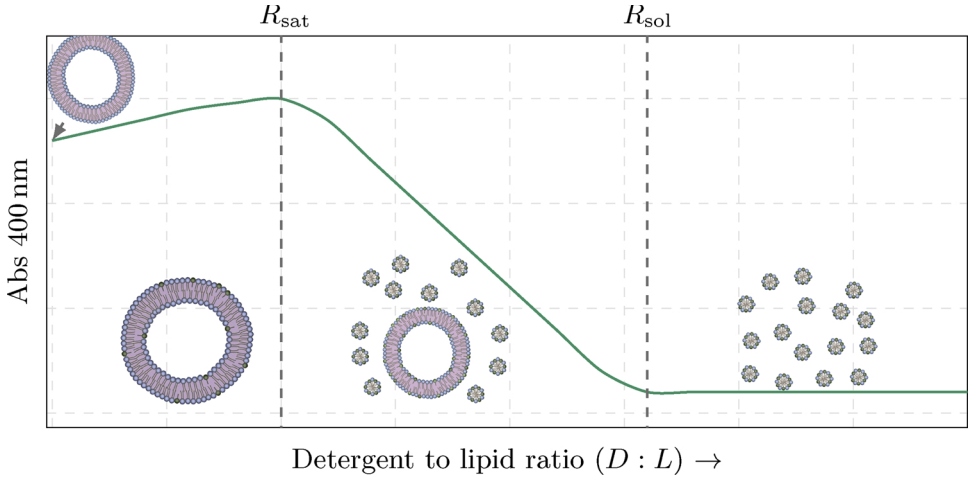

Fig. 2. Demonstration of morphological changes in detergent solubilization of liposomes observed throughout turbidity measurements with absorbance spectrophotometry recorded at 400 nm. In Stage I (left panel), detergent incorporates into lipid leaflets of the liposomes until the bilayer is saturated (R_{sat}). In Stage II (middle panel), increasing D:L leads to shrinking of liposome diameter and formation of detergent and lipid mixed-micelles. Stage III (right panel) is initiated with complete solubilization of liposomes into mixed-micelles (R_{sol}). Adapted from Seddon et al. [10].

using an Avanti Mini-Extruder system outfitted with a Whatman Nuclepore Track-Etch membrane (model 800309). All samples were extruded at room temperature. The lipid solution was passed 31 times through the membrane apparatus outfitted with 100 nm pore filters to form large unilamellar vesicles (LUVs). LUVs were used in subsequent experiments the day they were prepared.

2.3. Absorbance spectrophotometry

The composition-dependent equilibrium transition of liposomes in the presence of varying detergent concentrations can be described following a three-stage model. This model describes morphological changes that occur as the lipid bilayer is disrupted (solubilized) into micelles [8,9,13,14]. The stages of detergent-liposome interactions are depicted in Fig. 2. They are labeled (I) saturation (or onset of solubilization), (II) partial solubilization, and (III) full solubilization. The morphological changes are illustrated schematically moving along the graph with increasing detergent concentration (*x*-axis) and the observed absorbance using spectrophotometry (*y*-axis). Stage I is signified by partitioning and insertion of detergent monomers into the liposomal bilayer, which results in swelling of the liposomes and a concomitant increase in light scattering measured with a spectrophotometer. In Stage II, there is coexistence of detergent monomers, liposomes, and micelles containing a mixture of lipid and detergent molecules. Stage II is seen with decreasing observed absorbance. In Stage III, there is a complete dissociation of liposomes into mixed lipid–detergent micelles in which further detergent addition does not influence observed absorbance, thus Stage III is marked by a baseline absorbance. Saturation (R_{sat}) is the mass ratio of detergent to lipid at the maximum detergent concentration that liposome bilayer's can incorporate before mixed lipid–detergent micelles begin forming. It is seen as the transition point from Stage I to Stage II. Liposome solubilization (R_{sol}) is the mass ratio of detergent to lipid at the point of complete disruption of all lamellar phases. It is seen as the transition point from Stage II to Stage III. Previous studies indicate that the most successful protein incorporation occurs during the second stage of detergent-mediated solubilization [8,10,26]. It is, therefore, relevant to map these transitions. The detergent concentration necessary for the onset of each stage is influenced by lipid–lipid interactions within the bilayer, and lipid interactions with the surrounding aqueous environment. Variable lipid characteristics, such as charge, head group size, and length and degree of saturation of fatty acid chains, can be selected to influence membrane properties and solubilization [34].

In this work, the stages of solubilization with the detergent, TX, were determined for equillibrated liposomes. TX dilutions were prepared at 2.4–120 mg/ml and added to aliquots of liposomes in duplicate at detergent to lipids (D:L) ratios of 0–6 w/w. These were mixed 10 times using a pipette, and equilibrated at room temperature for 30 min. The final lipid concentration of all aliquots were 3.2 mg/ml. The absorbance of the lipid–detergent emulsions was measured at 400 nm using a Thermo-Scientific NanoDrop 2000C spectrophotometer at room temperature. Accompanying NanoDrop 2000 software was used in the UV-vis mode to do a full spectrum sweep between 190–840 nm to observe any sample placement issues, such as air bubbles, and record the absorbance at 400 nm. Three measurements were taken for each sample and averaged for a final absorbance at each D:L ratio. The data was then normalized to an initial liposome absorbance of 1. This procedure was replicated three times for each lipid composition and pH. The average of multiple runs was graphed with standard deviations to determine the affinity of detergent to each lipid composition and pH. Liposome saturation (R_{sat}) and solubilization (R_{sol}) were determined from the resulting absorbance versus D:L solubilization curves. R_{sat} was determined at the peak of the curve. R_{sol} was defined to be the first D:L less than or equal to the average of the last three data points plus standard deviation of 0.007. 0.007 was determined to be the instrument and samples margin of error by performing repeated measurements on the same sample.

2.4. Dynamic light scattering

Dynamic light scattering (DLS) was used to monitor a change in the size distribution of pure lipid liposomes and fully solubilized mixed-micelles. Samples were prepared in the same manner as for absorbance spectrometry with either no TX or at TX concentrations that resulted in detergent-to-lipid ratios above R_{sol} determined in absorbance experiments. Emulsions were given approximately 30 min to equilibrate prior to measuring the diameter and distribution in a Wyatt Technology DynaPro NanoStar fixed angle dynamic light scattering instrument. 10 µL samples at 3.33 mg lipid per ml were measured at 20 °C for 20 acquisitions of 10 s each. Samples were made in triplicate for each lipid mixture and buffer. The data was fit with the standard isotropic sphere model at optimal resolution and averaged over the independent preparations.

2.5. Isothermal titration calorimetry

To observe the binding affinity of detergent with liposomes and assess the change in enthalpy as the surfactant partitions lipid membranes, isothermal titration calorimetry (ITC) is considered a preferred method [35,36]. Following the protocol of Heerklotz et al. [37], adapted by Nirromand et al. [38], the characteristic heat signal under TX titration into preformed liposomes was observed using a VP-ITC instrument manufactured by MicroCal Inc. (Northampton, MA). To prepare samples, 4 mg/ml extruded liposomes and 154 mM TX solution

were degassed under reduced pressure with constant stirring for 10 min, slightly below the experimental temperature, at 23 °C. Following degassing, the calorimeter sample cell and injector-syringe chamber were loaded with 1.4 mL of the liposome solution and 300 μL of the detergent solution. A series of TX injections were made at 30 minute intervals following this sequence: 2.0, 3.0, 3.0, 3.0, 3.0, 4.0, 2.0, 3.0, 3.0, 2.0, 4.0, 4.0, 4.0, 4.0, 2.0, 3.0, 4.0, 3.0, 4.0, 3.0, 3.0, 3.0, 7.0, 4.0, 5.0, 5.0, 6.0, 4.0, 6.0, 4.0, 7.0, 6.0, 5.0, 7.0, 13.0, 10.0, 20.0, 22.0, 25.0, 25.0, 30.0 μL. This series of injections was chosen to optimize enthalpic data in regions of interest, i.e. near R_{sat} and R_{sol}. The change in applied heat to maintain a constant sample cell temperature was recorded and analyzed using VPViewer program. Integration of the heat signal describes the change in enthalpy for each injection.

3. Results and discussion

3.1. Turbidity evidence of mixed-lipid liposome disruption by TX

Turbidity changes in liposome solutions were quantified using optical absorbance with spectrophotometry at 400 nm at varying mass ratios of D:L for mixed-lipid vesicles with varying ratios of ePC and ePA. In this technique, absorbance decreases with decreasing particle size, and increases with increasing particle size (see Section 2.3). The curve is used to determine R_{sat} at the D:L ratio of the highest absorbance and R_{sol} at the D:L ratio initiating a baseline absorbance. As the initial amounts of detergent are added to the liposomes, detergent monomers penetrate the bilayers. In the lowest D:L ratio (0.12), the TX concentration is an order of magnitude above the detergent critical micelle concentration of 0.15 mg/ml in pure water. In Fig. 3, the curve shapes for mixtures of ePC and ePA are characteristic of general detergent association and break-down of liposomes. Here, the D:L ratios (R_{sat} and R_{sol}) that characterize the stages of solubilization are much lower for liposomes containing only ePC lipids, and are higher for liposomes containing any amount of ePA lipids. The intra-liposome mixing of lipids was confirmed with differential scanning calorimetry (Figure S1). In liposomes containing a mixture of both lipids, the D:L ratios at which the stages of solubilization occur are most similar to that of ePA-only liposomes. Additionally, the normalized absorbance at 400 nm in Stages I and II are also markedly higher for all ePA-containing samples than for ePC alone. In Stage III, the normalized absorbance is similar for all samples, marking the complete conversion of liposomes into mixed micelles. We also note that the liposomes had a similar starting diameter, as shown in Table 1. The average diameter of the stage III mixed-micelles was similar for all lipid compositions (Table 1 and Figure S2). These results confirm that liposomes were completely solubilized by TX detergent, but do not describe or provide evidence of changes of diameter during the process of detergent solubilization.

Fig. 4(a) shows the detergent to lipid ratios at peak liposomes saturation, R_{sat}, for the mixed-lipid liposomes (see Section 2.3). R_{sat} is plotted as a function of lipid composition with increasing percentage of ePA; the remaining is ePC. In Fig. 4, mixed-lipid liposomes containing only 25% conical ePA lipids incorporate nearly twice as much TX as cylindrical ePC liposomes alone. 50% ePA incorporates a similar concentration of TX as 25% ePA, whereas 75% and 100% ePA liposomes reach R_{sat} with even more TX.

In Fig. 4(b), R_{sol} is displayed for each lipid composition in Fig. 3. This is the ratio of detergent to lipid at the first point that liposomes are completely solubilized into mixed-micelles. R_{sol} is higher for 100% ePA than 100% ePC (0% ePA). Additionally, error bars are standard deviations and do not include instrumental or systematic error.

The difference in D:L ratios for saturating and solubilizing liposomes can be explained by the shape of each lipid. As seen in Fig. 1, ePC has a cylindrical shape and ePA has a conical shape. In the liposomes, of the order of 100 nm, the lipids interact as in a planar bilayer [23]. The cylindrical ePC lipids form a bilayer with cylinders stacked side-by-side with little space for TX to insert. Thus ePC liposomes reach R_{sat} and R_{sol} at low D:L ratios with little increase in normalized absorbance at R_{sat}. Conversely, ePA lipids have a conical shape that form gaps between the phospholipid heads in bilayers that more easily accept TX [1,39]. ePA-only liposomes reach R_{sat} and R_{sol} at the highest D:L ratios and a high normalized absorbance at R_{sat}. This shows there is significant swelling as TX is incorporated into ePA bilayers, and that ePA bilayers can take on more TX before disrupting into mixed-micelles. Mixed-lipid liposomes, with at least 25% or more conical ePA, have openings for TX to more easily incorporate into the bilayer resulting in liposomes behaving more similarly to ePA-only than ePC-only.

3.2. ITC evidence of mixed-lipid liposome disruption by TX

To gain understanding on the influence of ePA and ePC on TX solubilization, isothermal titration calorimetry (ITC) was performed. ITC was used to monitor the partition of detergent into bilayers, as well as the formation of mixed-micelle structures as detergent is titrated into a solution with pre-formed liposomes. The equilibrated processes of saturation and solubilization release and absorb net heat that were observed through changes in compensation heating power (Δp) required to maintain a fixed temperature. In Fig. 5, these transitions were observed for 100:0, 75:25, 0:100 ePC:ePA liposomes. 75:25 ePC:ePA mixed-lipid liposomes were chosen to observe if a similar trend in R_{sat} and R_{sol} at the low ePA concentration existed with ITC as with absorbance measurements in Section 3.1. The top row, shows the raw data of Δp applied during each injection of TX, which is always followed by an equilibration period. The injection volumes were varied to optimize the resolution in the R_{sat} region, as seen in previously published protocols [37,38]. The heat power curves throughout the titration exhibited the same characteristic solubilization shape, starting with a positive Δp

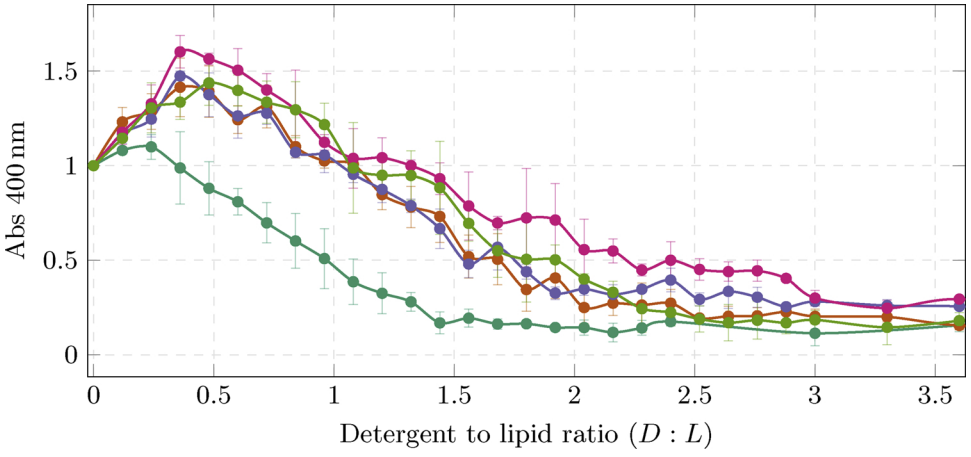

Fig. 3. Turbidity changes in mixed-lipid ePC:ePA liposomes at 100:0 (■),75:25 (■), 50:50 (■), 25:75 (■), and 0:100 (■) were induced by TX detergent addition and measured using absorbance spectrometry at 400 nm. Data-point connecting lines are shown as guides to the eye. The solubilization curves for liposomes containing more than 25% ePA reached a higher absorbance and were shifted right compared to ePC-only liposomes.

Table 1
Diameter of ePC:ePA mixed-lipid liposomes without TX and mixed-micelles with TX in Stage III of solubilization. This confirms a similar starting size for all lipid compositions and complete dissolution of liposomes at a higher D:L ratio than R_{sol}.

ePC:ePA Sample	100:0	75:25	50:50	25:75	0:100
Liposome d (nm)	121.7 ± 3.5	120.0 ± 2.7	118.7 ± 4.6	120.2 ± 1.5	126.1 ± 2.8
Mixed-Micelle d (nm)	17.8 ± 2.3	19.4 ± 1.4	19.7 ± 0.7	18.1 ± 5.3	19.9 ± 3.4

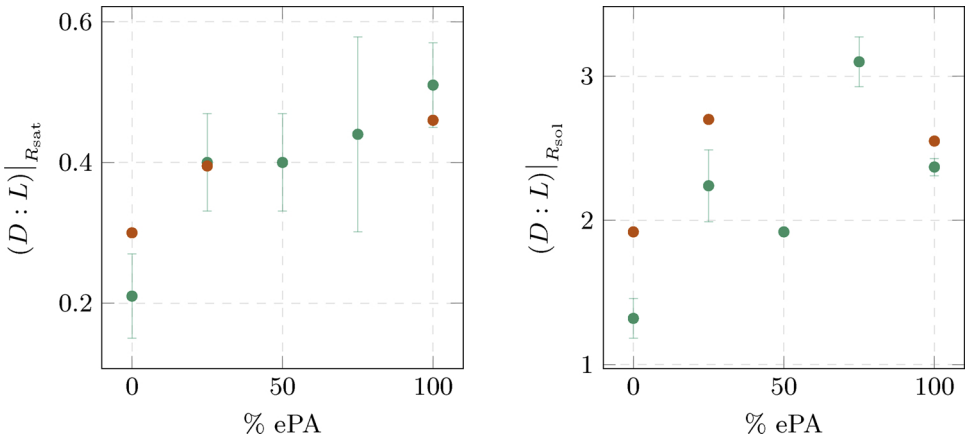

Fig. 4. D:L ratio at (a) R_{sat}, liposome saturation, and (b) R_{sol}, liposomes solubilization, for mixed ePC and ePA lipid liposomes. Values were obtained via absorbance spectrophotometry (■) and isothermal titration calorimetry (■). Results are displayed as % ePA, and the remainder is % ePC. Any amount of ePA observed increases the D:L ratio at R_{sat} and R_{sol}. The effect of PA is non-linear. As a percent increase, R_{sat} and R_{sol} increase more for low % ePA levels and then the effect does not increase as much for high % ePA levels.

endothermic region (Stage I), followed by a negative Δp exothermic region (Stage II), and lastly, a small, positive Δp endothermic region (Stage III), barely or not reached for 25 and 100% ePA samples due to chamber volume limitations. Stages I, II, and III mentioned here correspond to the stages described by the absorbance solubilization curve, shown in Fig. 2. In Stage I, Δp for both 25 and 100% ePA liposomes was higher and the stage persisted over more TX titrations than for 100% ePC liposomes. This corresponds to observations made in Sections 3.2 and 3.3 in which higher concentrations of TX are required to transition to Stage II. As the time-based injections varied in volume, it is useful to look at D:L throughout the titrations in the bottom row of Fig. 5.

In Fig. 5(bottom row), raw heat power data was used to calculate the heats of injection per mole of TX as a function of D:L on a weight basis. The D:L transitions for R_{sat} were determined after the highest Q peak started to monotonically decrease. For R_{sol}, a logistic function with a linear offset, $y = A\left(1 - \frac{1}{1+e^{\frac{x-\mu}{\sigma}}}\right) + c$, was fit to the monotonic portion of the data starting at the inversion point (minimum) in the forth quadrant. R_{sol} was found at $y = 0$ of the resulting fit. For 100:0, 75:25, and 0:100 ePC:ePA, R_{sat} is 0.30, 0.40, and 0.46 w/w D:L, and R_{sol} is 1.92, 2.70, and 2.55 w/w D:L. The data is shown in Fig. 4 for

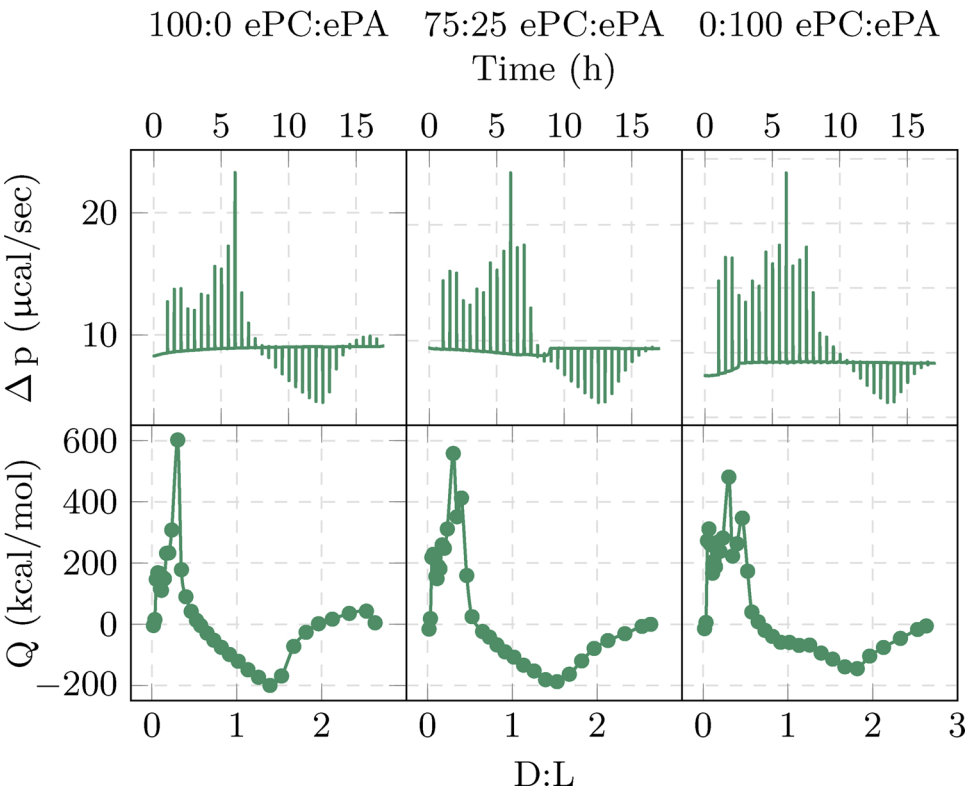

Fig. 5. Isothermal titration calorimetry for solubilization of preformed liposomes with stepwise titrations of TX. Liposomes made with (left to right) 100:0, 75:25, and 0:100 ePC:ePA. (top) Raw data of compensation heat power, Δp (µcal/s), versus time in hours. (bottom) Heats of injection, Q (kcal/mol TX), versus D:L ratio (w/w). The solid lines are again a guide to the eye. The ITC data show that the response to TX titration of mixed lipid liposomes containing 25% ePA is more similar to that of 100% ePA than 0% ePA.

comparison to the absorbance results. These values are at slightly higher than absorbance spectrometry observations in Section 3.1. Nevertheless, the trend of both absorbance and ITC data sets are the same, in which pure ePC reaches R_{sat} and R_{sol} at the lowest D:L of all the samples. Also, the R_{sat} and R_{sol} values of 25% or more ePA lipids are closer to that of ePA-only samples.

3.3. Triton X-100 association with ePA as a function of pH and charge

The primary differences between ePC and ePA lipids are charge and head group size and shape. This leads to different overall lipid shapes and packing within bilayers. The ePA headgroup is smaller than the ePC headgroup, as discussed above this lends to an overall conical shape of ePA lipids and a cylindrical shape of ePC lipids. Since ePA, a charged lipid, liposomes require a higher concentration of TX to solubilize than ePC liposomes, the effect of the charge on solubilization was examined by adjusting the pH, and thus, the lipid ionization, as depicted in Fig. 1. Absorbance solubilization curves of 0:100 ePC:ePA liposomes at pH 6, 7 and 8 can be seen in Fig. 6. ePA liposomes at pH 8 are saturated and solubilized at the lowest D:L ratio of the tested buffers. ePA liposomes at pH 7 are saturated and solubilized at a higher D:L, and lastly, ePA liposomes at pH 6 are saturated and solubilzed at the highest D:L. The absorbance curves shift to the right as the pH decreases for ePA liposomes. Additionally, the absorbance maxima increases slightly with decreasing pH. The change in peak absorbance at 400 nm compared to the pristine extruded liposome is 0.58, 0.44, and 0.38 for increasing pH from 6 to 7 to 8. This means that decreasing the pH allows the liposomes to swell more before the onset of solubilization occurs. R_{sat} and R_{sol} were determined as described above and are graphed in the inset of Fig. 6. A roughly linear relationship is seen for R_{sat} and R_{sol}, and as pH increases, the D:L ratio required to achieve these states decreases. The D:L ratios at R_{sat} and R_{sol} were approximately 1.8 times higher at pH 6 than at pH 8. As with mixed-lipid liposomes, the average diameter of the prepared liposome and fully solubilized mixed-micelles was similar (Table S2 and Figure S3).

Changes in D:L at R_{sat} and R_{sol}, and changes in maximum absorbance of ePA at varying pH, show that ePA charge affects the interaction of TX with the bilayers. The ionization potential in Fig. 1, shows that at a lower pH, ePA is in a less negative state. At the lowest pH observed, pH 6, the R_{sat}, R_{sol} and maximum absorbance of liposomes was the highest measured. At this pH, ePA is less negatively charged than at pH 7 and 8, and thus there are fewer counter-ions present in the bilayer. The decrease in counter-ions makes the shape of ePA more conical [40]. As discussed in Section 3.1, we see a strong correlation between lipid shape and R_{sat}/R_{sol}, and here, the more conical ePA has more mismatches in the bilayer. This enables higher concentrations of TX to be incorporated in the liposomes before disrupting into mixed-micelles. Conversely, ePA at the highest pH observed, pH 8, is in a more negatively charged state and has more counter-ions present. The increased counter-ions lend to a less conical shape, which increases the resistance to TX incorporation into the bilayer. Further, the solubilization curve of ePC liposomes is also shown in Fig. 6. It is seen that the cylindrical shape of the lipids in liposomes are saturated and solubilized with less TX than conically shaped ePA lipids.

4. Conclusions

TX is a non-ionic amphiphilic molecule with a long hydrophilic polyethylene oxide chain and a bulky aromatic hydrocarbon group. It was incorporated into liposomes of varying compositions made of ePC and ePA lipids. Absorbance spectrometry shows that ePC liposomes are solubilized with significantly less TX than ePA-only and mixed-lipid ePC:ePA liposomes at mass ratios of 25:75, 50:50, or 75:25. The TX response of liposomes containing any amount of ePA tested here more closely resembles that of 100% ePA than 100% ePC liposomes. Additionally, during ITC, the heat power response to TX titration of 25% ePA liposomes more closely resembles 100% ePA than 100% ePC. Thus, the influence of ePA, even at low concentrations, makes ePC liposomes less sensitive to disruption by TX.

The differences in ePA and ePC interactions in liposomes with TX are explained by lipid shape in Fig. 7. The structure of ePC lipids consists of a mobile, zwitterionic phosphotidyl choline head group and a combination of saturated and unsaturated fatty acid chains, as seen in Fig. 1(a). The overall structure of the lipid is cylindrical. The liposome size used here, which is greater than 100 nm in diameter, has little curvature effect on the individual lipid interactions. This enables efficient packing of cylindrical lipids, as seen in Fig. 7(first row). The packing of cylinders increases the difficulty of TX to incorporate into the liposome. This results in reduced swelling at R_{sat}, lower possible incorporation of TX into bilayers, and liposomes that transition to mixed-micelles at lower ratios of TX to lipid. Conversely, the structure of ePA lipids is made up of a small, immobile phosphatic acid head group and a combination of saturated and unsaturated fatty acid chains, seen in Fig. 1(b). The generally accepted structure is conical [29], which creates defects in the bilayer between neighboring conical lipids and favors the incorporation of TX into the liposome bilayers, Fig. 7(second and third rows). Easier incorporation of TX, allows the liposomes to accommodate higher concentrations of TX and swell more before disrupting into mixed-micelles. The influence of the conical ePA shape also has a drastic effect on R_{sat} when ePA is mixed with ePC in liposomes. The three ratios of ePC:ePA mixed-lipid liposomes observed showed that the conical shape significantly enhanced the maximum uptake of liposomes before disruption, Fig. 7(second row). While the arrangement of ePC and ePA lipids within the bilayer is not yet known,

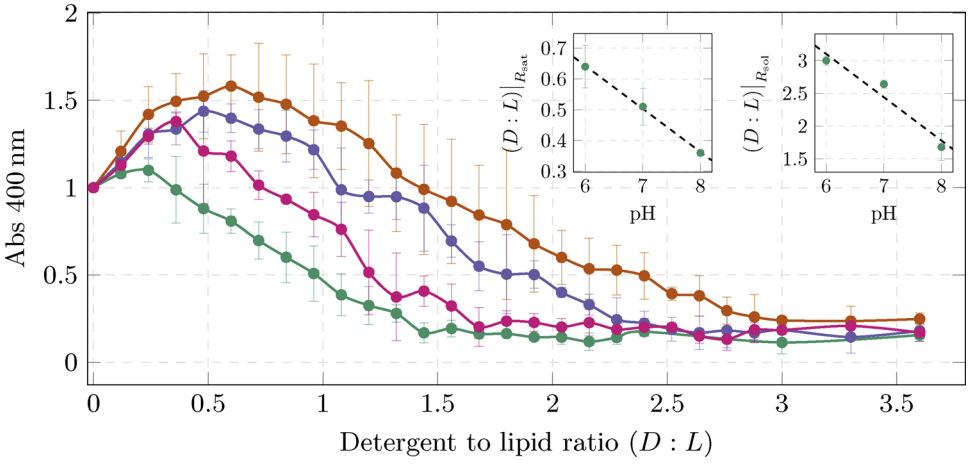

Fig. 6. Turbidity changes in ePA liposomes at pH 6 (■), pH 7 (■), and pH 8 (■) and ePC liposomes (■), induced by detergent addition and measured using absorbance spectrometry at 400 nm. The solid lines are a guide to the eye. Additionally, the D:L ratios at liposome saturation (left inset) and solubilization (right inset) for ePA at pH 6, 7 and 8. ePA liposomes at pH 6 incorporated higher concentrations of TX than at pH 8; additionally there was a linear increase in R_{sat} and $R_{sol}$with pH.

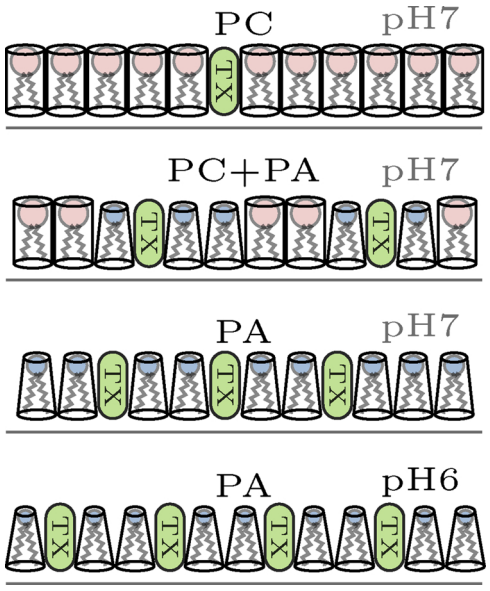

Fig. 7. Illustration of the influence of lipid shape in the outer liposomes leaflet on TX incorporation into varying lipid bilayers. In the first row, the cylindrical shape of PC incorporates the lowest concentration of TX at R_{sat} and R_{sol}. In the second row, addition of conical shape PA lipids into the PC bilayer promotes incorporation of a higher TX concentration. In the fourth row, PA at pH 6 has a more conical shape than pH 7 (third row), which enables uptake of higher TX concentrations.

our data suggest the addition of even 25% conical lipid drastically increases the density of defects in the bilayers and increases R_{sat} and maximum swelling before bilayer disruption.

Additionally, we probed the influence of lipid charge in ePA on TX solubilization by varying the pH. The net charge of ePA transitions from −1 to −2 between pH 6 and 8, as seen in Fig. 1(b). TX absorbance solubilization curves of ePA liposomes at pH 6, 7, and 8, seen in Fig. 6, show that there is a linear relationship between charge and R_{sat}/R_{sol}. More negatively charged ePA liposomes are saturated and solubilized at lower D:L ratios. Decreased ease of detergent saturation and solubilization in more negatively charged bilayers can be explained by increased counter-ion affinity at the head groups, which alters the shape of the lipids in the bilayers. PA is known to have a conical shape due to the small phosphatidic acid head group. Addition of a counter-ion at higher pH (i.e. pH 6 vs. pH 7, and pH 7 vs. pH 8) causes an increase in head group size and makes the overall lipid shape less conical, as seen in Fig. 7(third row). Less conical ePA lipids, pH 8, pack together more tightly, which reduces insertion of TX into liposomes. Conversely, more conical ePA lipids,like at pH 6, have more defects in liposome layers that ease the incorporation of TX Fig. 7(fourth row). As discussed with ePC liposomes, fewer defects in the bilayers result in a lower association of TX monomers before liposomes begin restructuring into mixed-micelles.

In summary, based on our results we found that a lipid shape model can be used to explain detergent solubilization characteristics of single-lipid and mixed-lipid liposomes, which is a necessary early step in creating native-like liposomes that incorporate proteins for functional purpose.

Author contributions

Conception and design: S.C., P.F.; Acquisition of data: S.C.; Analysis and interpretation of data: S.C., M.A., S.S., P.F.; Drafting of manuscript: S.C.; Critical revision: S.C., M.A., S.S., P.F.

Funding

This research was funded through the GAANN Program of the US Department of Education, Award Number P200A120191.

Conflicts of interest

The authors declare no conflict of interest.

Acknowledgments

We thank Graham J. Taylor, T & T Scientific, for his consultation and assistance in performing differential scanning calorimetry. We also thank Ed Wright, BCMB UTK, for assistance in isothermal titration calorimetry measurements.

Appendix A. Supplementary data

Supplementary data associated with this article can be found, in the online version, at https://doi.org/10.1016/j.colsurfb.2019.110609.

References

[1] V.V. Kumar, Complementary molecular shapes and additivity of the packing parameter of lipids (chain length/phase preference/theory), Biophysics 1 (January) (1991) 444–448, https://doi.org/10.1073/pnas.88.2.444.
[2] H. Hauser, G. Poupart, The Structure of Biological Membranes, 2nd ed., CRC Press, Boca Raton, Fla, 2005.
[3] B.J. Harris, X. Cheng, P. Frymier, All-atom molecular dynamics simulation of a photosystem, J. Phys. Chem. B 118 (2014) 11633–11645, https://doi.org/10.1021/jp507157e.
[4] I.J. Iwuchukwu, M. Vaughn, N. Myers, H. O'Neill, P. Frymier, B.D. Bruce, Self-organized photosynthetic nanoparticle for cell-free hydrogen production, Nat. Nanotechnol. 5 (1) (2010) 73–79, https://doi.org/10.1038/nnano.2009.315.
[5] B.J. Harris, X. Cheng, P. Frymier, Structure and function of photosystem I-[FeFe] hydrogenase protein fusions: an all-atom molecular dynamics study, J. Phys. Chem. B 120 (4) (2016) 599–609, https://doi.org/10.1021/acs.jpcb.5b07812.
[6] R.K. Le, M. Raeeszadeh-Sarmazdeh, E.T. Boder, P.D. Frymier, Sortase-mediated ligation of PsaE-modified photosystem I from synechocystis sp. PCC 6803 to a conductive surface for enhanced photocurrent production on a gold electrode, Langmuir 31 (3) (2015) 1180–1188, https://doi.org/10.1021/la5031284.
[7] R.K. Le, B.J. Harris, I.J. Iwuchukwu, B.D. Bruce, X. Cheng, S. Qian, W.T. Heller, H. O'Neill, P.D. Frymier, Analysis of the solution structure of Thermosynechococcus elongatus Photosystem I in n-dodecyl-β-d-maltoside using small-angle neutron scattering and molecular dynamics simulation, Arch. Biochem. Biophys. 550–551 (2014) 50–57, https://doi.org/10.1016/j.abb.2014.04.005.
[8] J. Knol, K. Sjollema, B. Poolman, Detergent-mediated reconstitution of membrane proteins, Biochemistry 37 (46) (1998) 16410–16415, https://doi.org/10.1021/bi981596u.
[9] M.-T. Paternostre, M. Roux, J.-L. Rigaud, Mechanisms of membrane protein insertion into liposomes during reconstitution procedures involving the use of detergents. 1. Solubilization of large unilamellar liposomes (prepared by reverse-phase evaporation) by Triton X-100, Octyl Glucoside, and Sodium, Biochemistry 27 (8) (1988) 2677–2688, https://doi.org/10.1021/bi00408a007.
[10] A.M. Seddon, P. Curnow, P.J. Booth, Membrane proteins, lipids and detergents: not just a soap opera, Biochim. Biophys. Acta – Biomembr. 1666 (1–2) (2004) 105–117, https://doi.org/10.1016/j.bbamem.2004.04.011.
[11] D. Lichtenberg, Characterization of the solubilization of lipid bilayers by surfactants, BBA – Biomembranes 821 (3) (1985) 470–478, https://doi.org/10.1016/0005-2736(85)90052-5.
[12] J.L. Rigaud, B. Pitard, D. Levy, Reconstitution of membrane proteins into liposomes: application to energy-transducing membrane proteins, BBA – Bioenergetics 1231 (3) (1995) 223–246, https://doi.org/10.1016/0005-2728(95)00091-V.
[13] D. Lichtenberg, H. Ahyayauch, A. Alonso, F.M. Goñi, Detergent solubilization of lipid bilayers: a balance of driving forces, Trends Biochem. Sci. 38 (2) (2013) 85–93, https://doi.org/10.1016/j.tibs.2012.11.005.
[14] U. Kragh-hansen, M. Maire, J.V. Møller, The mechanism of detergent solubilization of liposomes and protein-containing membranes, Biophys. J. 75 (6) (1998) 2932–2946, https://doi.org/10.1016/S0006-3495(98)77735-5.
[15] H. Ahyayauch, M.I. Collado, A. Alonso, F.M. Goñi, Lipid bilayers in the gel phase become saturated by Triton X-100 at lower surfactant concentrations than those in the fluid phase, Biophys. J. 102 (11) (2012) 2510–2516, https://doi.org/10.1016/j.bpj.2012.04.041.
[16] A. Dickey, R. Faller, Examining the contributions of lipid shape and headgroup charge on bilayer behavior, Biophys. J. 95 (6) (2008) 2636–2646, https://doi.org/10.1529/biophysj.107.128074.
[17] H. Ahyayauch, B. Larijani, A. Alonso, F.M. Goñi, Detergent solubilization of phosphatidylcholine bilayers in the fluid state: influence of the acyl chain structure, Biochim. Biophys. Acta – Biomembr. 1758 (2) (2006) 190–196, https://doi.org/10.

1016/j.bbamem.2006.01.016.
[18] M.A. Partearroyo, A. Alonso, F.M. Goñi, M. Tribout, S. Paredes, Solubilization of phospholipid bilayers by surfactants belonging to the Triton X series: effect of polar group size, J. Colloid Interface Sci. 178 (1) (1996) 156–159, https://doi.org/10.1006/jcis.1996.0103.
[19] T.M. Bayer, G.D. Werner, E. Sackmann, Solubilization of DMPC and DPPC vesicles by detergents below their critical micellization concentration: high-sensitivity differential scanning calorimetry, Fourier transform infrared spectroscopy and freeze-fracture electron microscopy reveal two interac, BBA – Biomembranes 984 (2) (1989) 214–224, https://doi.org/10.1016/0005-2736(89)90219-8.
[20] J.R. Henriksen, T.L. Andresen, L.N. Feldborg, L. Duelund, J.H. Ipsen, Understanding detergent effects on lipid membranes: a model study of lysolipids, Biophys. J. 98 (10) (2010) 2199–2205, https://doi.org/10.1016/j.bpj.2010.01.037.
[21] A. Hildebrand, K. Beyer, R. Neubert, P. Garidel, A. Blume, Solubilization of negatively charged DPPC/DPPG liposomes by bile salts, J. Colloid Interface Sci. 279 (2) (2004) 559–571, https://doi.org/10.1016/j.jcis.2004.06.085.
[22] L. Sun, J. Mao, Y. Zhao, C. Quan, M. Zhong, S. Fan, Coarse-grained molecular dynamics simulation of interactions between cyclic lipopeptide Bacillomycin D and cell membranes, Mol. Simul. 7022 (October) (2017) 1–13, https://doi.org/10.1080/08927022.2017.1384632.
[23] A. Pizzirusso, A. De Nicola, G.J. Sevink, A. Correa, M. Cascella, T. Kawakatsu, M. Rocco, Y. Zhao, M. Celino, G. Milano, Biomembrane solubilization mechanism by Triton X-100: a computational study of the three stage model, Phys. Chem. Chem. Phys. 19 (44) (2017) 29780–29794, https://doi.org/10.1039/c7cp03871b.
[24] D. Lichtenberg, R.J. Robson, E.A. Dennis, Solubilization of phospholipids by detergents structural and kinetic aspects, BBA – Rev. Biomembr. 737 (2) (1983) 285–304, https://doi.org/10.1016/0304-4157(83)90004-7.
[25] J.R. Silvius, Solubilization and functional reconstitution of bioemembrane components, Annu. Rev. Biophys. Biomol. Struct. 21 (1992) 323–348, https://doi.org/10.1146/annurev.bb.21.060192.001543.
[26] J. Cladera, J.L. Rigaud, H. Bottin, M. Dunach, Functional reconstitution of Photosystem I reaction center from cyanobacterium Synechocystis sp PCC 6803 into liposome using a new reconstitution procedure, J. Bioenerg. Biomembr. 28 (6) (1996) 503–515, https://doi.org/10.1007/BF02110440.
[27] Z. Gombos, H. Wada, Z. Varkonyi, D.A. Los, N. Murata, Characterization of the Fad12 mutant of Synechocystis that is defective in, 412 acyl-lipid desaturase activity Zoltan, Biochim. Biophys. Acta 1299 (1996) 117–123.
[28] A.G. Lee, Lipid–protein interactions in biological membranes: a structural perspective, Biochim. Biophys. Acta – Biomembr. 1612 (1) (2003) 1–40, https://doi.org/10.1016/S0005-2736(03)00056-7.
[29] J.N. Israelachvili, S. Marcelja, R.G. Horn, Physical principles of membrane organization, Q. Rev. Biophys. 13 (2) (1980) 121–200.
[30] J.J.H. Shin, C.J.R. Loewen, Putting the pH into phosphatidic acid signaling, BioMed Cent. Biol. 85 (9) (2011) 1–10, https://doi.org/10.1186/1741-7007-9-85.
[31] K. Lähdesmäki, O.H. Ollila, A. Koivuniemi, P.T. Kovanen, M.T. Hyvönen, Membrane simulations mimicking acidic pH reveal increased thickness and negative curvature in a bilayer consisting of lysophosphatidylcholines and free fatty acids, Biochim. Biophys. Acta – Biomembr. 1798 (5) (2010) 938–946, https://doi.org/10.1016/j.bbamem.2010.01.020.
[32] T. Zhang, S.L. Brantley, D. Verreault, R. Dhankani, S.A. Corcelli, H.C. Allen, Effect of pH and salt on surface pKa of phosphatidic acid monolayers, Langmuir 34 (2018) 530–539, https://doi.org/10.1021/acs.langmuir.7b03579.
[33] F. Szoka Jr., D. Papahadjopoulos, Comparative properties and methods of preparation of lipid vesicles (liposomes), Annu. Rev. Biophys. Bioeng. 9 (1980) 467–508, https://doi.org/10.1146/annurev.bb.09.060180.002343.
[34] W. Dowhan, M.V. Bogdanov, E. Mileykovskaya, Functional roles of lipids in membranes, in: N.D. Ridgway, R.S. McLeod (Eds.), Biochemistry of Lipids, Lipoproteins and Membranes, 6th ed., Elsevier, 2015, pp. 1–40, , https://doi.org/10.1016/B978-0-444-63438-2.00001-8.
[35] P. Draczkowski, D. Matosiuk, K. Jozwiak, Isothermal titration calorimetry in membrane protein research, J. Pharm. Biomed. Anal. 87 (2014) 313–325, https://doi.org/10.1016/j.jpba.2013.09.003.
[36] M. Deleu, J.M. Crowet, M.N. Nasir, L. Lins, Complementary biophysical tools to investigate lipid specificity in the interaction between bioactive molecules and the plasma membrane: a review, Biochim. Biophys. Acta – Biomembr. 1838 (12) (2014) 3171–3190, https://doi.org/10.1016/j.bbamem.2014.08.023.
[37] H. Heerklotz, A.D. Tsamaloukas, S. Keller, Monitoring detergent-mediated solubilization and reconstitution of lipid membranes by isothermal titration calorimetry, Nat. Protoc. 4 (5) (2009) 686–697, https://doi.org/10.1038/nprot.2009.35.
[38] H. Niroomand, D. Mukherjee, B. Khomami, Tuning the photoexcitation response of cyanobacterial Photosystem I via reconstitution into proteoliposomes, Sci. Rep. 7 (865) (2017) 1–13, https://doi.org/10.1038/s41598-017-02746-5.
[39] D.A.N. Morris, R. McNeil, F.J. Castellino, J.K. Thomas, Interaction of lysophosphatidylcholine with phosphatidylcholine bilayers, Biochim. Biophys. Acta 599 (1980) 380–390.
[40] E.E. Kooijman, V. Chupin, B. de Kruijff, K.N. Burger, Modulation of membrane curvature by phosphatidic acid and lysophosphatidic acid, Traffic 4 (3) (2003) 162–174, https://doi.org/10.1034/j.1600-0854.2003.00086.x.